Coverage Contact Control of Benzoxazole-Based SAMs to Enhance the Operational Performance of Perovskite Nanocrystal Light–Emitting Diodes

Alexis Villanueva-Antolí, Laia Marín-Moncusí, Carlos E. Puerto-Galvis, Rafael S. Sánchez, Jorge Simancas, Eva M. Barea, Jhonatan Rodriguez-Pereira, Carina Pareja-Rivera, Andrés F. Gualdrón-Reyes, Emilio Palomares, Eugenia Martínez-Ferrero,* and Iván Mora-Seró*

Perovskite light–emitting diodes (PeLEDs) have emerged as a prominent topic within optoelectronic research. Despite remarkable advancements, this technology still faces challenges that must be addressed for successful commercialization. Typical device architectures employ PEDOT:PSS as hole transporting material (HTM). However, besides its expensive cost, PEDOT:PSS has been reported to cause issues with efficiency and long-term stability. Molecular self-assembled monolayers (SAMs) have arisen as potential HTMs, not just to overcome these drawbacks but to enhance the interface properties and performance of LEDs. This technology has been efficiently applied in PeLEDs, but its use in devices based on perovskite nanocrystals (PNCs) remain underexplored. In this work, two benzoxazole derivatives have been analyzed as SAMs to conform the hole selective contact in CsPbBr$_3$ PNCs-based LEDs. The devices demonstrate improved optoelectronic properties compared to the reference composed of PEDOT:PSS, attributed to a suitable band alignment and an enhanced charge injection. Furthermore, optimizing the deposition technique of SAMs on the conducting substrate by dip- or spin-coating has allowed the preparation of efficient LEDs exhibiting external quantum efficiencies (EQEs) up to 6.8% with 300 s of operational stability. This research aims to provide extensive insights into applying SAMs to design PeLEDs with improved carrier mobility.

1. Introduction

Halide perovskites (HPs) have been extensively studied as semiconductors for optoelectronic applications due to their exceptional attributes, including emission with high color purity and easy tunability, as well as solution processability and elevated defect tolerance, establishing them as one of the most revolutionary photoactive materials.[1,2] Moreover, the remarkable capabilities of HPs can be further enhanced when synthesized as colloids. In this form, perovskite nanocrystals (PNCs) exhibit superior optical properties than their polycrystalline counterparts due to improved crystallinity and surface energy phase stabilization.[3–6] In addition to their application in the fabrication of solar cells and other kinds of optoelectronic devices,[7–9] HPs have been effectively employed in LEDs, achieving external quantum efficiency (EQE) values

A. Villanueva-Antolí, R. S. Sánchez, J. Simancas, E. M. Barea,
C. Pareja-Rivera, I. Mora-Seró
Institute of Advanced Materials (INAM)
Universitat Jaume I (UJI)
Avenida de Vicent Sos Baynat, s/n, Castellón de la Plana 12071,
Castellón, Spain
E-mail: sero@uji.es
L. Marín-Moncusí, C. E. Puerto-Galvis, E. Palomares, E. Martínez-Ferrero
Institute of Chemical Research of Catalonia (ICIQ-BIST iCERCA)
Avda. Països Catalans, 16, Tarragona 43007, Spain
E-mail: emartinez@iciq.es

L. Marín-Moncusí
Departament d'Enginyeria Electrònica, Elèctrica i Automàtica
Universitat Rovira i Virgili
Avda. Països Catalans, 26, Tarragona 43007, Spain
J. Rodriguez-Pereira
Center of Materials and Nanotechnologies
Faculty of Chemical Technology
University of Pardubice
Nam. Cs. Legii 565, Pardubice 53002, Czech Republic
J. Rodriguez-Pereira
Central European Institute of Technology
Brno University of Technology
Purkynova 123, Brno 61200, Czech Republic
A. F. Gualdrón-Reyes
Facultad de Ciencias, Instituto de Ciencias Químicas, Isla Teja
Universidad Austral de Chile
Valdivia 5090000, Chile
E. Palomares
Catalan Institution for Research and Advanced Studies (ICREA)
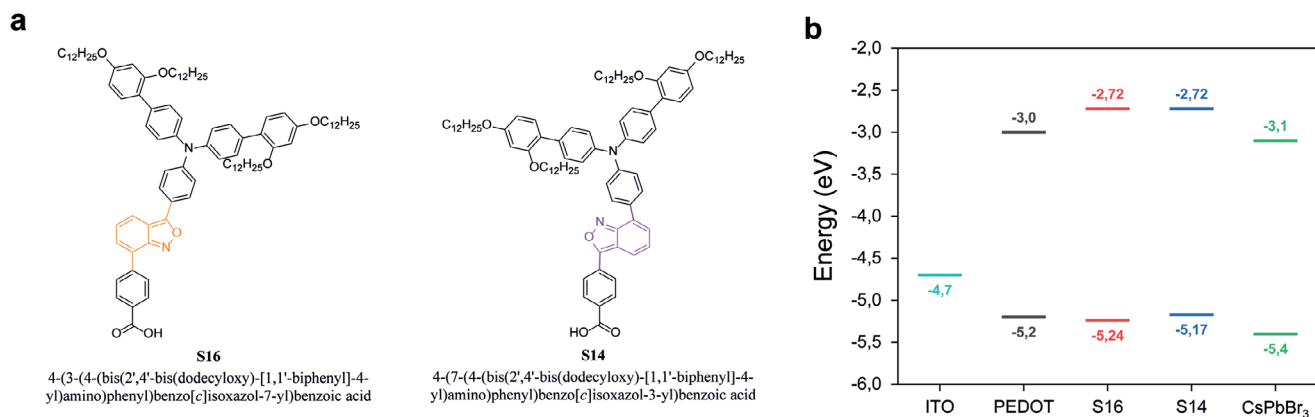Barcelona 08010, Spain

Figure 1. a) Molecular structures of the SAMs; b) ITO work function, S14 and S16 HOMO (bottom line) and LUMO (top line) levels, PEDOT and CsPbBr$_3$ valence (bottom line) and conduction (top line) bands.[37,41,42]

higher than 25%, 28%, and 18% for red-, green-, and blue-emitting devices, respectively.[10–12] Despite the widespread study of PNCs as photoactive materials, there are still some critical issues related to halide migration, charge balance, and heat generation in operando, which hinder the stability of devices based on this technology.[13–16] Nevertheless, alongside efficiency, extending the lifetime of LEDs is one of the most pivotal factors for their successful commercialization. Therefore, ensuring device stability is of paramount importance.

Along with the active layer, the other constituents in the configuration play a crucial role in the performance of the LEDs.[17] Regarding the charge transfer, one of the most common HTM is PEDOT:PSS (Poly(3,4-ethylenedioxythiophene)-poly(styrenesulfonate), hereafter referred to as PEDOT), due to their excellent conductivity, high transparency, and easy solution processability.[18,19] However, despite these characteristics, the hygroscopic and acidic nature of PEDOT makes it prone to absorb water and oxidize the adjacent layers within the structure, which is detrimental to the operational performance of the device.[20] Moreover, additional processes are sometimes conducted to prepare highly conductive PEDOT.[21,22] These procedures complicate the material processing and increase costs, ultimately affecting the overall price of the device and hindering the commercialization of this technology.[23,24] In this regard, the use of SAMs has emerged as a promising alternative to avoid the hydrophile-associated instability, acidity, and cost of PEDOT, while increasing interface properties and ultimately device performance.

Molecules able to produce SAMs constitute a class of organic compounds that can form ordered arrangements through chemisorption onto the surface of a material. Moreover, SAM molecules can be designed and synthesized by selecting their components (i.e., the anchor group, the linker, and the substituents) to tune their optical and electrical properties, conferring exceptional adaptability to different interfaces.[25–29] In this context, SAMs can be deposited on conducting substrates to modulate their surface energy and the work function of the electrode, achieving a better band alignment with other components of a device and favoring the charge transport.[30] Moreover, the careful design and selection of the functional groups in contact with the photoactive layer can induce changes in the layer formation and

the interfacial charge dynamics.[31] Furthermore, the deposition of the molecules is also relevant as can affect device properties. Dip-coating (DC) and spin-coating (SC) are the most widely used liquid-phase deposition techniques at laboratory scale.[32] While the former consists of immersing the substrate in a saturated solution of SAM molecules enough time to let the molecules attach to the surface, forming really a monolayer, the latter is based on dispensing the solution on the substrate at certain spinning velocity. The spin-coating method is preferred due to its easy and rapid workup.[33,34] Their versatility, low-cost manufacturing, and easy processability, turn SAMs into a potential replacement for PEDOT in the design of devices. Although there are many reports where SAMs have been successfully employed in solar cells or, more recently, in LEDs, the effect of SAMs on the electronic properties of devices based on PNC films, especially appealing for LEDs, has not been studied in depth.[31,35,36]

In this work, we have analyzed the suitability of two benzoxazole derivatives (S14 and S16, **Figure 1**) as SAMs for acting as hole-selective contacts in fabricating green-emitting LEDs based on CsPbBr$_3$ PNCs.[37] We achieved a proper band alignment between the SAMs terminal moiety and the PNCs, favoring the charge injection to the active layer and, hence, improving the operational performance of the device compared to the reference LEDs using PEDOT. Furthermore, we have compared two different deposition methods to prepare SAM films (i.e., spin-coating and dip-coating) and their impact on the device's efficiency and stability. In this context, we elucidate that the use of SC promotes homogeneous layers and better charge injection to the PNCs active layer, yielding LEDs with an EQE averaging of 6.8 ± 1.2% and an operational lifetime of 305 s. This contribution provides new findings on optimizing the hole-selective material to fabricate more efficient and stable LEDs.

2. Results and Discussion

Two benzoxazole derivatives, designated S14 and S16, have been functionalized with a carboxylic acid group and a N-(2′,4′-bis(dodecyloxy)-[1,1′-biphenyl]-4-yl)-2′,4′-bis(dodecyloxy)-N-phenyl-[1,1′-biphenyl]-4-amine unit.[37] The highly conjugated benzoxazole group promotes the extension of the π-system along the molecule, enhancing its conductivity.[38] In addition,
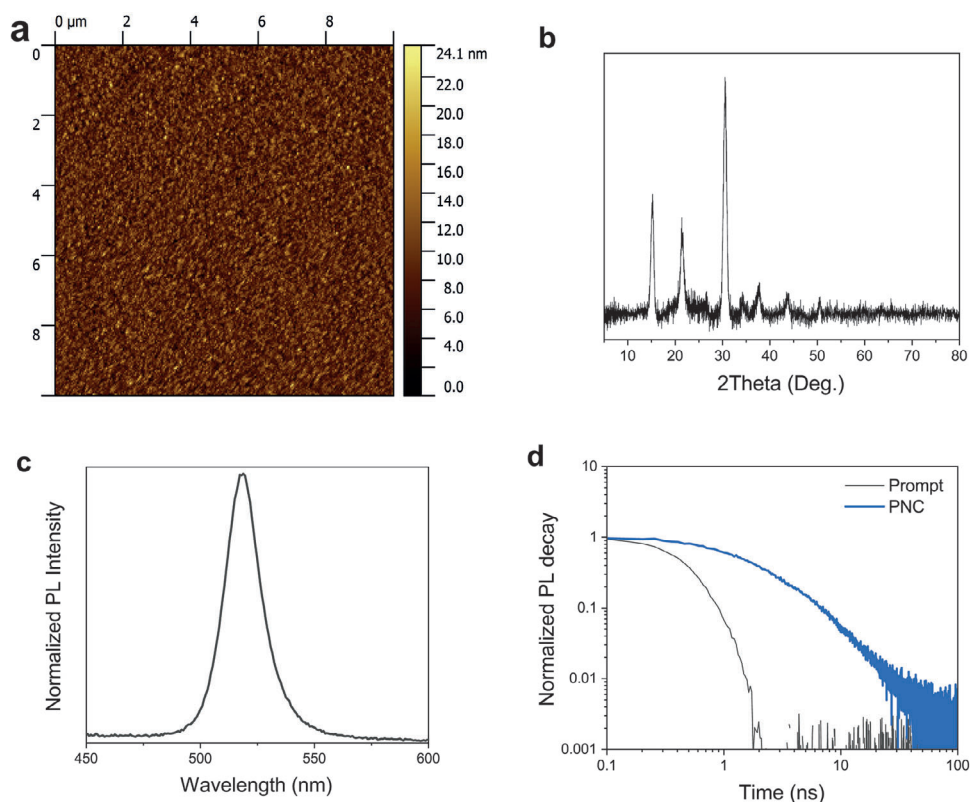
2400884 (2 of 7)

Figure 2. a) CsPbBr$_3$ NCs film on top of glass/ITO substrate characterization by AFM; b) XRD; c) PL spectrum; and d) TRPL decay spectrum, (λ_{exc} = 405 nm). Note: the "Prompt" data in d) represents the equipment response, measured using a non-emissive colloidal silica dispersion (LUDOX AS-40).

the carboxylic acid is one of the most used anchoring groups for conductive oxides, providing a solid attachment of the molecule to the indium-doped tin oxide (ITO) surface due to the formation of mono and bidentate covalent bindings at room temperature without compromising the charge transfer.[26] Moreover, the alkoxy groups within the amine act as the terminal moiety which interacts with the PNCs. Some studies pinpoint the use of alkoxy groups to effectively passivate the trap states within the perovskite layer effectively.[39,40] In **Figure 1**, the structure of the S14 and S16 is represented, as well as the energy levels of these molecules and those of the ITO, PEDOT, and CsPbBr$_3$ NCs. It is worth highlighting that the HOMO levels of PEDOT, S14, and S16 are very close to the perovskite one, favoring the carrier injection into the active layer. Nevertheless, the LUMO levels are higher for the S14 and S16 compared with the PEDOT, which is close to the nanocrystal band. This characteristic suggests that S14 and S16 may act as more effective electron-blocking layer (EBL) than PEDOT, facilitating the recombination of excitons in the active layer and promoting the radiative emission of the perovskite.

These molecules have been deposited on top of ITO-coated glass substrates to analyze the surface properties of the SAMs used as hole-selective contacts, compared with conventional glass/ITO/PEDOT films. The formation of the SAMs film on ITO surface has been monitored by X-ray photoelectron spectroscopy (XPS), see Figure S1 (Supporting Information). The quantitative results are presented in Table S1 (Supporting Information), where the signal corresponding to nitrogen (N) in the substrates

with S14 and S16 can be observed. In addition, there is a shift toward higher binding energies for the oxygen (O), indium (In), and tin (Sn) signals in all SAM samples compared to ITO, confirming the deposition of these molecules on the substrate surface, see Figure S1 (Supporting Information). The clear detection of the Sn and In signals, unlike those in the PEDOT film, suggests that the SAM molecules form very thin layers on the ITO.

CsPbBr$_3$ PNCs have been synthesized by hot-injection method, purified, and redispersed in a concentration of 10 mg mL^{-1} in hexane, see Experimental Section in Supporting Information for detailed description, based on the methodology presented by Protesescu and colleagues,[43] with modifications.[44] Figure S2a (Supporting Information) shows the optical characterization of the PNCs dispersion by absorption and photoluminescence (PL) measurements, obtaining a phtoluminescenc quantum yield (PLQY) ≈62% after the purification of the material. The typical morphology and corresponding size distribution, 9.8 ± 1.8 nm, can be seen in the inset of Figures S2a and S3 (Supporting Information), respectively. Furthermore, PL decay lifetime is shown in Figure S2b (Supporting Information), with their corresponding parameters summarized in Table S2 (Supporting Information), obtaining an average lifetime (τ_{avg}) of 9.6 ns. All these parameters are in good agreement with previously reported for CsPbBr$_3$ PNCs.[45]

The characterization of PNCs has also been conducted after deposition as thin film. Atomic force microscopy (AFM) measurements, presented in **Figure 2a**, reveal a homogeneous distribution across the entire surface of the film. Additionally,

the X-ray diffraction (XRD) diffractogram shown in Figure 2b confirms the orthorhombic phase (ICSD 97851) of the perovskite. The optical spectroscopic properties have been measured, through PL spectrum, depicted in Figure 2c; along with the PL decay lifetimes of the films obtained from time-resolved photoluminescence (TRPL), illustrated in Figure 2d and Table S2 (Supporting Information). The root mean square (RMS) roughness of the surface is summarized in Table S3 (Supporting Information).[46,47] Since the material's characterization is also appropriately correlated with the values reported, the perovskite has been employed to prepare LEDs. Finally, we have estimated the hole mobility (μ_h) from hole-only devices with the architecture ITO/SAMs/PNCs/MoO3/Ag by the space-charge-limited current (SCLC) method. The description of the method is given in the Supporting Information. The μ_h was found to be 6.24×10^{-7} and 5.75×10^{-7} cm^2 V^{-1} s^{-1} for the devices prepared with S14 and S16, respectively.

Following, we have analyzed the interaction between the SAMs and the PNCs by depositing the perovskite on top of the dip-coated molecules. Figure S4 (Supporting Information) displays the AFM images for the films ITO/PEDOT/PNC, ITO/S14/PNC, and ITO/S16/PNC, respectively, while the tabulated values of their RMS roughness analysis can be found in Table S3 (Supporting Information). From the images, it can be observed that the surface morphology is homogeneous and very similar between the different samples. However, the variance in the roughness suggests a smoother layer formation in the case of S14, probably due to a better packing of the SAM layer.[38] In addition, to assess the SAMs' wettability, we measured the contact angle of the films with water and hexane since this last solvent is the one composing the perovskite solution. In the case of hexane, the contact angle was extremely low (<5°). Moreover, the evaporation rates exceed the drop spreading over the surface, making it impossible to measure an equilibrium contact angle precisely. This shallow contact angles evidence an extremely high wettability of the perovskite solution solvents over the HTM layers. Otherwise, we could measure the water contact angle with PNC films deposited on top of the different HTMs, Figure S5a–c (Supporting Information). We observed that the contact angle of perovskite on top of both SAMs was very similar (≈55.7°) and lower than the PEDOT/PNC film (63.8°). In this context, diverse studies, such as the Wenzel or the pinning models, correlate the film roughness with the water contact angle, evidencing smoother surface for lower angles.[48–50] These results agree with the AFM characterization and confirm a better formation of the PNCs film on top of the SAMs. The XRD patterns, Figure S6a (Supporting Information), show that the orthorhombic phase of the perovskite is maintained for all the samples without any significant change in the diffraction patterns. Moreover, PL spectra also remain unchanged, while PL lifetimes show minor differences for the three kinds of HTMs, Figure S6b,c and Table S2 (Supporting Information), respectively. These results highlight the differing nature of the PEDOT and the SAMs, also suggesting that the linker orientation in the SAM structure influences packing of the self-assembled layer and the formation of the perovskite film.

Concerning the fabrication of LEDs, Figure S7 (Supporting Information) illustrates the device architecture consisting of ITO/HTM/PNC/PO-T2T/LiF/Al, with the HTM being either PEDOT, S14, or S16, all pivotal for the manufacturing of emissive LEDs.[17,51] We first studied the performance of devices with the different SAMs deposited by DC. Optoelectrical characterization of the different devices is presented in **Figure 3** and summarized in Table S4 (Supporting Information). From Figure 3a, it can be inferred that using SAMs as hole-selective contacts promotes the charge injection, resulting in higher current densities at low voltages and increased luminance in comparison with reference PEDOT. However, SAM-based devices show relatively high standard deviations, indicating lower reproducibility in both cases. This phenomenon is emphasized in Figure 3c, where the LEDs composed by SAMs yield higher efficiencies than the reference with PEDOT but also significant variability that can be assigned to heterogeneities on the surface coverage. Additionally, the EL spectra in Figure 3b exhibit an emission peak at 515 nm for all types of devices. At the same time, the International Commission on Illumination (CIE) plot in Figure S8 (Supporting Information) reveals minimal differences in the emission color. Figure 3d presents the EL evolution over time of the different samples, with their corresponding potential shown in Figure S9 (Supporting Information). S16 exhibits a slightly longer half-lifetime (t$_{50}$, time in which initial luminance drops to 50%) compared to S14, both surpassing considerably the stability of the reference devices. Conversely, PEDOT devices exhibit more uniform decay, probably because of the rapid degradation of these LEDs.[36] In light of these results, SAM-based devices demonstrate enhanced performance compared to PEDOT. As mentioned before, this can be ascribed to the decrease in the concentration of defects at the interface that improves the charge injection into the active layer and a proper band alignment of SAMs acting as both, HTM and improved EBL respect PEDOT. Specifically, the band alignment detailed in Figure S7b (Supporting Information) reveals that while the HOMO levels of the HTMs are comparable, the LUMO level of SAMs is significantly higher than that of PEDOT, which closely aligns with the perovskite. This difference in alignment prevents electron leakage from the perovskite layer, promoting efficient recombination within the emissive layer and contributing to the superior EQE observed in SAM-based devices. Therefore, we primarily attribute this improvement to the electron-blocking properties of SAMs, though the suppressed diffusion of acids and ions from PEDOT could also play a secondary role in device stability. Moreover, although the standard deviation is moderately elevated, devices composed of S14 present a subtle enhancement in the optoelectronic properties, compared to S16 ones, both in luminance and efficiency, while stability is slightly shorter. A possible explanation for the improved electronic properties of LEDs based on S14 could be the bonding of the anchor unit to the oxazole unit of the linker core, which has higher electron density than the benzyl, thereby promoting the charge transport between the anchor and the functionalized terminal groups of the SAMs. This is also reflected in slightly higher hole mobility, and in the increase of In and Sn atoms bonded to the SAM, as indicated by the shift of the corresponding peaks after SAM deposition, which is more pronounced in the case of S14, Figure S1 (Supporting Information). Additionally, the smoother film formed by S14 in comparison to S16 and PEDOT, Table S3 (Supporting Information), suggests a better arrangement of this compound on the ITO surface, promoting the interaction with the active layer and enhancing the overall performance of the device.
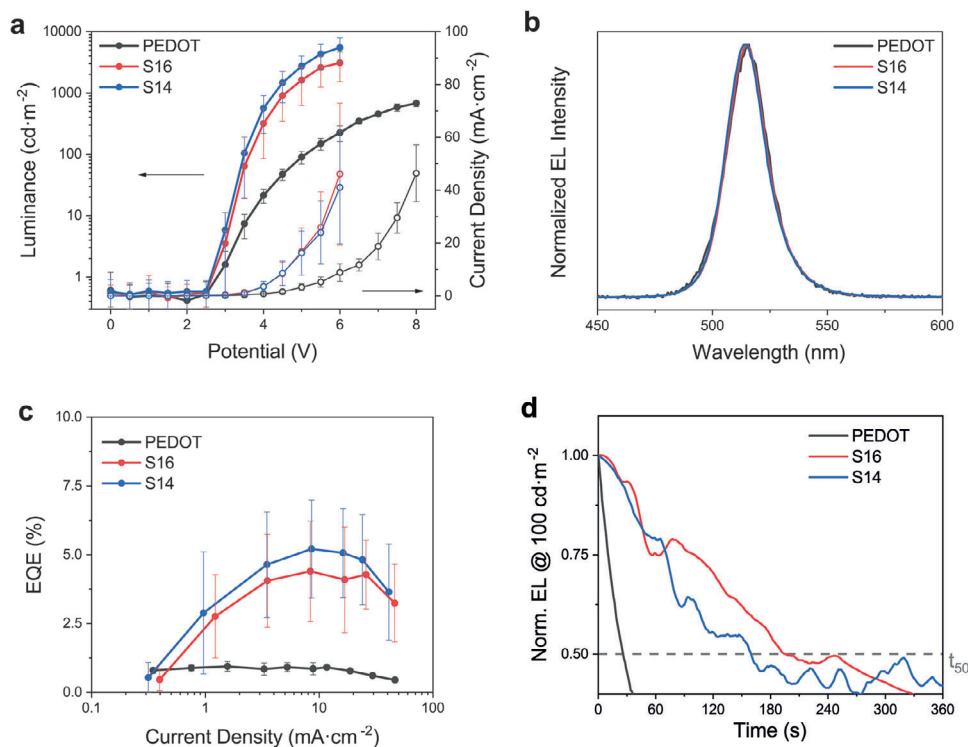
ADVANCED
SCIENCE NEWS

www.advancedsciencenews.com

ADVANCED
MATERIALS
INTERFACES
Open Access

www.advmatinterfaces.de

Figure 3. a) J–V (empty dots) and Lum-V (filled dots) curves, b) EL spectra, c) EQE, and d) t_{50} at 100 cd m^{-2} initial luminance for devices HTM-based in S14 and S16 deposited by DC and PEDOT.

From the results discussed above, indeed, the molecular design of SAMs influences the optoelectronic properties of the final LEDs; however, to acquire additional insights into the effect of SAMs as hole-selective contacts, we have studied the impact of the deposition method of these molecules on device performance. Similarly to the previous section, the deposition of the SAMs on top of the ITO has been first confirmed by XPS, Figure S1 and Table S1 (Supporting Information). It can be seen the increase of the binding energies of In-O and Sn-O bond signals of ITO/SAM films compared to PEDOT, evidencing the attachment of the SAMs on the substrate surface, as well as the nitrogen presence.

The following step has been the deposition of PNCs on top of the HTM. As in the former section, it has been analyzed by AFM, Figure S10 (Supporting Information), revealing a similar trend to the one previously described for dip-coated films. The surface morphology is homogeneous for both materials; however, it is noteworthy that although the roughness is quite similar for S14 films deposited by DC and SC, indicating smooth layers in both methods, the S16 spin-coated films exhibit smoother surfaces than dip-coated ones, Table S3 (Supporting Information). So far, these observations suggest that SC facilitates a better arrangement of S16 molecules than DC, which promotes more uniform films. Moreover, the contact angle with water, Figure S5d,e (Supporting Information), is very similar to their dip-coated counterparts. PNCs crystallinity has been assessed by XRD, Figure S11a (Supporting Information), observing the conservation of the orthorhombic structure. Again, steady-state and time-resolved PL spectra, presented in Figure S11b,c (Supporting Information) respectively, follow the same trend previ-

ously observed, obtaining longer lifetimes for S16 than for S14, Table S2 (Supporting Information). Nevertheless, in comparison to DC, the spin-coated samples have shorter average lifetimes. Since short-lifetime components are usually ascribed to excitonic recombination, while long-lifetime components are related to exciton-defect interactions, it is feasible that there are fewer defects in spin-coated layers, decreasing the overall average lifetime.[45]

The fabrication of the LEDs has been conducted with identical architecture, Figure S7 (Supporting Information), and in the same manner as their dip-coated analogous, with the only difference being the SAMs deposition by SC. **Figure 4** compares the performance of devices based in S14 DC and SC. While the maximum luminance and the current density, Figure 4a, are slightly lower for spin-coated devices, they present higher efficiency and half-lifetime, reaching 6.8 ± 1.2% of EQE and a t_{50} of 305 s, Figure 4c,d respectively. It is worth highlighting that, in contrast to the dip-coated counterpart, the stability curve shape is remarkably uniform. Moreover, the S14-based devices exhibit an initial EQE overshoot, typically associated with ion migration toward interfaces, which suggests an enhanced charge injection. These findings are consistent with the results observed from second measurements of the device efficiency. As shown in Figure S12 (Supporting Information), the I–V curves for dip-coated devices exhibit noticeable differences between the first and second scans, whereas these variations are less pronounced for the spin-coated counterparts. Nonetheless, a decrease in EQE is observed for both types of devices upon repeated measurements. These observations may suggest that ion migration likely contributes to the performance drop.
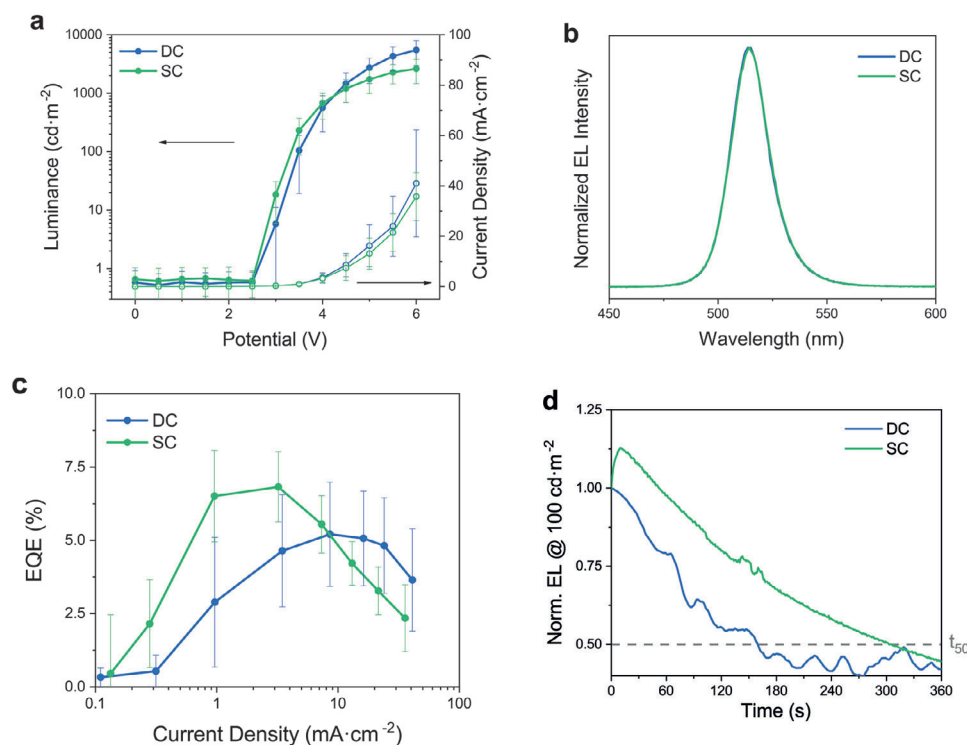
Figure 4. a) *J–V* (empty dots) and Lum-V (filled dots) curves, b) EL spectra, c) EQE, and d) t_{50} at 100 cd m^{-2} initial luminance for S14-based devices deposited by DC and SC.

Additionally, these devices present a lower standard deviation, indicating a better reproducibility for spin-coated LEDs, probably due to the better homogeneity in the film formation.[34] Figure S13 (Supporting Information) compares DC and SC devices based on S16, depicting an analogous effect to the one observed in S14. Moreover, an image of all the LED variations in operando is presented in Figure S14 (Supporting Information). Therefore, the results obtained suggest that the spin-coating deposition technique provides more homogeneous coverage, enhancing the performance and reproducibility of SAM-based LEDs.

3. Conclusion

In the present study, we have evaluated two benzoxazole derivatives able to form SAM as substitutes for the widely used PEDOT. The devices, including SAMs within their architecture, have demonstrated enhanced performance in terms of efficiency and stability in comparison with PEDOT hole injecting layer. The influence of the structural design of SAMs extends beyond the terminal moieties linked to the perovskite, with subtle distinctions in behaviors between SAMs differentiated solely by the inversion of the linker orientation. Furthermore, we have assessed the effect of SAMs deposition by comparing dip- and spin-coating techniques, with the latter yielding significant improvement in efficiency, stability, and reproducibility. By optimizing the preparation of the perovskite LEDs using a suitable SAM based on a functionalized benzoxazole derivative deposited via spin-coating, we have achieved a maximum EQE up to 6.8 ± 1.2% with t_{50} of 305 s, which is competitive with the current state of the art for this kind of configuration. These results continue to underscore the

notable potential of SAMs within LED design based in perovskite nanocrystals.

Supporting Information

Supporting Information is available from the Wiley Online Library or from the author.

Conflict of Interest

The authors declare no conflict of interest.

Data Availability Statement

The data that support the findings of this study are openly available in [zenodo.org] at [https://doi.org/10.5281/zenodo.14511544], reference number [14511544].

[1] K. Wang, D. Yang, C. Wu, M. Sanghadasa, S. Priya, *Prog. Mater. Sci.* **2019**, *106*, 100580.

[2] C. He, X. Liu, *Light. Sci. Appl.* **2023**, *12*, 15.

[3] H. Oga, A. Saeki, Y. Ogomi, S. Hayase, S. Seki, *J. Am. Chem. Soc.* **2014**, *136*, 13818.

[4] T. Yamada, T. Handa, Y. Yamada, Y. Kanemitsu, *J. Phys. D Appl. Phys.* **2021**, *54*, 383001.

[5] S. T. Brinck, F. Zaccaria, I. Infante, *ACS Energy Lett.* **2019**, *4*, 2739.

[6] A. F. Gualdrón-Reyes, S. Masi, I. Mora-Seró, *Trends Chem* **2021**, *3*, 499.

[7] M. A. Green, A. Ho-Baillie, H. J. Snaith, *Nat. Photonics* **2014**, *8*, 506.

[8] H. Wang, Y. Sun, J. Chen, F. Wang, R. Han, C. Zhang, J. Kong, L. Li, J. Yang, *Nanomaterials* **2022**, *12*, 4390.

[9] L. Lei, Q. Dong, K. Gundogdu, F. So, *Adv. Funct. Mater.* **2021**, *31*, 2010144.

[10] J. Jiang, Z. Chu, Z. Yin, J. Li, Y. Yang, J. Chen, J. Wu, J. You, X. Zhang, *Adv. Mater.* **2022**, *34*, 2204460.

[11] J. S. Kim, J. M. Heo, G. S. Park, S. J. Woo, C. Cho, H. J. Yun, D. H. Kim, J. Park, S. C. Lee, S. H. Park, E. Yoon, N. C. Greenham, T. W. Lee, *Nature* **2022**, *611*, 688.

[12] Y. Jiang, C. Sun, J. Xu, S. Li, M. Cui, X. Fu, Y. Liu, Y. Liu, H. Wan, K. Wei, T. Zhou, W. Zhang, Y. Yang, J. Yang, C. Qin, S. Gao, J. Pan, Y. Liu, S. Hoogland, E. H. Sargent, J. Chen, M. Yuan, *Nature* **2022**, *612*, 679.

[13] X. Li, M. Haghshenas, L. Wang, J. Huang, E. Sheibani, S. Yuan, X. Luo, X. Chen, C. Wei, H. Xiang, G. Baryshnikov, L. Sun, H. Zeng, B. Xu, *ACS Energy Lett.* **2023**, *8*, 1445.

[14] T. Fang, T. Wang, X. Li, Y. Dong, S. Bai, J. Song, *Sci. Bull.* **2021**, *66*, 36.

[15] Q. Dong, L. Lei, J. Mendes, F. So, *J. Phys. Mater.* **2020**, *3*, 012002.

[16] L. Kong, X. Zhang, C. Zhang, L. Wang, S. Wang, F. Cao, D. Zhao, A. L. Rogach, X. Yang, *Adv. Mater.* **2022**, *34*, 43.

[17] K. M. M. Salim, E. Hassanabadi, S. Masi, A. F. Gualdrón-Reyes, M. Franckevicius, A. Devižis, V. Gulbinas, A. Fakharuddin, I. Mora-Seró, *ACS Appl. Electron. Mater.* **2020**, *2*, 2525.

[18] A. Kumar, C. Zhou, *ACS Nano* **2010**, *4*, 11.

[19] F. Zhi-Hui, H. Yan-Bing, S. Quan-Min, Q. Li-Fang, Y. Li, Z. Lei, X.-J. Liu, T. Feng, Y.-S. Wang, X. Rui-Dong, *Phys. B* **2010**, *19*, 38601.

[20] A. Rana, A. Kumar, S. Chand, R. K. Singh, *J. Appl. Phys.* **2019**, *125*, 053102.

[21] L. V. Lingstedt, M. Ghittorelli, H. Lu, D. A. Koutsouras, T. Marszalek, F. Torricelli, N. I. Crăciun, P. Gkoupidenis, P. W. M. Blom, *Adv. Electron. Mater.* **2019**, *5*, 3.

[22] L. Bießmann, N. Saxena, N. Hohn, M. A. Hossain, J. G. C. Veinot, P. Müller-Buschbaum, *Adv. Electron. Mater.* **2019**, *5*, 2.

[23] S. H. Jeong, S. Ahn, T. W. Lee, *Macromol. Res.* **2019**, *27*, 2.

[24] O. Carr, G. Gozzi, L. F. Santos, R. M. Faria, D. L. Chinaglia, *Transl. Mater. Res.* **2015**, *2*, 015002.

[25] A. Ulman, *Chem. Rev.* **1996**, *96*, 1533.

[26] S. P. Pujari, L. Scheres, A. T. M. Marcelis, H. Zuilhof, *Angew. Chem., Int. Ed.* **2014**, *53*, 6322.

[27] Q. Jiang, Z. Chu, P. Wang, X. Yang, H. Liu, Y. Wang, Z. Yin, J. Wu, X. Zhang, J. You, *Adv. Mater.* **2017**, *29*, 1703852.

[28] C. E. Puerto Galvis, D. A. González Ruiz, E. Martínez-Ferrero, E. Palomares, *Chem. Sci.* **2023**, *15*, 1534.

[29] W. Li, E. Martínez-Ferrero, E. Palomares, *Mater. Chem. Front.* **2023**, *8*, 681.

[30] Z. Yi, X. Li, Y. Xiong, G. Shen, W. Zhang, Y. Huang, Q. Jiang, X. R. Ng, Y. Luo, J. Zheng, W. L. Leong, F. Fu, T. Bu, J. Yang, *Interdiscip. Mater.* **2024**, *3*.

[31] S. Kumari, J. G. Sánchez, M. Imran, E. Aktas, D. A. González, L. Manna, E. Martínez-Ferrero, E. Palomares, *J. Mater. Chem. C* **2023**, *11*, 3788.

[32] F. Ali, C. Roldán-Carmona, M. Sohail, M. K. Nazeeruddin, *Adv. Energy Mater.* **2020**, *10*, 2002989.

[33] K. Choi, H. Choi, J. Min, T. Kim, D. Kim, S. Y. Son, G. W. Kim, J. Choi, T. Park, *Sol. RRL* **2020**, *4*, 1900251.

[34] M. Schultes, N. Giesbrecht, J. Küffner, E. Ahlswede, P. Docampo, T. Bein, M. Powalla, *ACS Appl. Mater. Interfaces* **2019**, *11*, 12948.

[35] M. Gedda, D. Gkeka, M. I. Nugraha, A. D. Scaccabarozzi, E. Yengel, J. I. Khan, I. Hamilton, Y. Lin, M. Deconinck, Y. Vaynzof, F. Laquai, D. D. C. Bradley, T. D. Anthopoulos, *Adv. Energy Mater.* **2023**, *13*, 2201396.

[36] C. Zhang, S. Mariotti, L. K. Ono, C. Ding, K. Mitrofanov, C. Zhang, S. Yuan, P. Ji, J. Zhang, T. Wu, R. Kabe, Y. Qi, *J. Mater. Chem. C* **2023**, *11*, 2851.

[37] L. Marin-Moncusí, C. E. Puerto-Galvis, E. Martínez-Ferrero, E. Palomares, *ChemComm* **2024**, https://doi.org/10.1039/x0xx00000x.

[38] C. Partes, C. Yildirim, S. Schuster, M. Kind, J. W. Bats, M. Zharnikov, A. Terfort, *Langmuir* **2016**, *32*, 11474.

[39] E. Arkan, E. Yalcin, M. Unal, M. Z. Y. Arkan, M. Can, C. Tozlu, S. Demic, *Mater. Chem. Phys.* **2020**, *254*, 123435.

[40] C. Huang, W. Fu, C. Z. Li, Z. Zhang, W. Qiu, M. Shi, P. Heremans, A. K. Y. Jen, H. Chen, *J. Am. Chem. Soc.* **2016**, *138*, 2528.

[41] D. Xu, S. Wu, Y. Zhao, X. Xu, G. He, Q. Wan, L. Li, *RSC Adv.* **2020**, *10*, 17653.

[42] H. Dong, S. Pang, Y. Zhang, D. Chen, W. Zhu, H. Xi, J. Chang, J. Zhang, C. Zhang, Y. Hao, *Nanomaterials* **2018**, *8*, 9.

[43] L. Protesescu, S. Yakunin, M. I. Bodnarchuk, F. Krieg, R. Caputo, C. H. Hendon, R. X. Yang, A. Walsh, M. V. Kovalenko, *Nano Lett.* **2015**, *15*, 3692.

[44] R. S. Sánchez, A. Villanueva-Antolí, A. Bou, M. Ruiz-Murillo, I. Mora-Seró, J. Bisquert, *Adv. Mater.* **2023**, *35*, 11.

[45] H. Chen, A. Guo, J. Zhu, L. Cheng, Q. Wang, *Appl. Surf. Sci.* **2019**, *465*, 656.

[46] K. Enomoto, R. Oizumi, N. Aizawa, T. Chiba, Y. J. Pu, *J. Phys. Chem. C* **2021**, *125*, 19368.

[47] L. Jiang, Z. Fang, H. Lou, C. Lin, Z. Chen, J. Li, H. He, Z. Ye, *Phys. Chem. Chem. Phys.* **2019**, *21*, 21996.

[48] C. Caddeo, D. Marongiu, S. Meloni, A. Filippetti, F. Quochi, M. Saba, A. Mattoni, *Adv. Mater. Interfaces* **2019**, *6*, 1801173.

[49] R. N. Wenzel, *Ind. Eng. Chem.* **1936**, *28*, 988.

[50] A. Giacomello, L. Schimmele, S. Dietrich, *Proc. Natl. Acad. Sci. U.S.A.* **2016**, *113*, E262.

[51] T. C. Almeida da Silva, R. S. Sánchez, J. A. Alberola-Borràs, R. Vidal, I. Mora-Seró, B. Julián-López, *Energy Environ. Mater.* **2024**, 12810.